Journal of Catalysis 276 (2010) 306–313

Contents lists available at ScienceDirect

Journal of Catalysis

journal homepage: www.elsevier.com/locate/jcat

The reaction mechanism of the high temperature ammonia oxidation to nitric oxide over $LaCoO_3$

Gregory Biausque, Yves Schuurman *

Institut de recherches sur la catalyse et l'environnement de Lyon, IRCELYON, CNRS, Université Lyon 1, UMR 5256, 2 Avenue Albert Einstein, F-69626 Villeurbanne, France

ARTICLE INFO

Article history:
Received 30 July 2010
Revised 21 September 2010
Accepted 22 September 2010

Keywords:
Temporal analysis of products
Nitrous oxide
Oxygen exchange
Perovskites

ABSTRACT

Perovskites are promising catalysts for oxidation reactions. Good NO selectivity is reported for the oxidation of ammonia into nitric oxide over $LaCoO_3$. More interestingly over this catalyst very little N_2O is produced, which makes it a potential candidate for industrial ammonia oxidation. In order to further develop perovskite catalysts, an understanding of the reaction mechanism is necessary. Steady-state, TAP and oxygen exchange experiments over $LaCoO_3$ have been carried out. A reaction mechanism that describes the product distribution (NO, N_2O and N_2) as a function of the oxidation degree of the catalyst has been proposed. The reaction proceeds by a Mars and Van Krevelen mechanism. NO and N_2O are formed through parallel routes from ammonia via surface nitroxyl (HNO) species. Formation of nitrogen occurs through at least three routes. Decomposition of both reaction products NO and N_2O leads to N_2, the latter decomposition being the fastest. The third route to N_2 consists of the reaction of adsorbed ammonia with short-lived oxygen surface species, such as peroxide or superoxide species.

1. Introduction

Nitric acid is one of the most utilized nitrogen containing compounds in the world. It is a commodity chemical for the production of fertilizers, nylon, explosives and all organic compounds involving nitration.

Its industrial production proceeds through ammonia oxidation with air into nitric oxide at high temperatures (>1073 K) and short contact times (10^{-4}–10^{-3} s) over platinum metal group (PGM) alloy gauzes via the Ostwald process [1]. Nitric oxide is further oxidized at low temperature to a mixture of nitrogen dioxide and dinitrogen tetroxide (N_2O_4) and these molecules react with water to yield nitric acid.

The key step in this process is the ammonia oxidation reaction. NO selectivity over PGM gauzes is in the range of 94–96%, but the catalysts' costs are high due to the high price of PGM's and the platinum losses through volatilization during the oxidation process. In addition, recent regulations require the abatement of N_2O, a greenhouse gas with a very long life time (120 years) and a global warning potential (GWP) 310 times higher than CO_2. Selectivity to N_2O over PGM gauzes is 1–2%. Currently, several different solutions within a nitric acid plant are put in place to decompose or reduce N_2O [2,3].

A more cost-effective way to tackle both issues is to replace the PGM catalysts by an oxide-based catalyst that does not produce N_2O. Research on oxides [3–8] shows that they are good catalysts for ammonia oxidation, especially cobalt oxide (Co_3O_4 spinel), iron oxide (α-Fe_2O_3) and chromium oxide.

Nitric oxide selectivity over oxides is comparable to that over PGM but the nitrous oxide selectivity is lower than over PGM catalysts. However, oxides suffer from low activity and insufficient stability. In some ammonia plants, cobalt-based bulk oxide monolith catalysts have replaced a part of the PGM gauze [7].

Crystalline mixed metal oxides have also been investigated and they seem to offer an interesting alternative. In this group, perovskites are attractive materials as they show good performance and offer large range of materials through substitution and doping. Appropriate formulation of these oxides leads to easy tailoring of many desirable properties such as valence state of transition metal ion, binding energy and diffusion of oxygen in the lattice and conducting properties of the solid.

In order to improve the performance of these materials, an understanding of the reaction mechanism and kinetics is indispensable. Few studies report on these issues over oxide materials for the high temperature ammonia oxidation [3,9,10].

Wu and co-workers [11] have compared the NO selectivity over A substituted (Ca, Sr) $LaMnO_3$, $LaCoO_3$ and $LaFeO_3$ perovskites. They proposed a mechanism involving adsorbed oxygen surface species (classifying the reaction of the supra facial type) and the formation of "HNO" as an intermediate species. However, they did not explain the formation N_2O nor did they take into account consecutive reactions of NO and N_2O.

Pérez-Ramírez and Kondratenko [12] has shown, in the first TAP study of ammonia oxidation over oxides, the participation of lattice

* Corresponding author. Fax: +33 4 78 44 53 99.
E-mail address: yves.schuurman@ircelyon.univ-lyon1.fr (Y. Schuurman).

0021-9517/$ - see front matter © 2010 Elsevier Inc. All rights reserved.
doi:10.1016/j.jcat.2010.09.022

oxygen of pure metal oxides (Fe_2O_3, Cr_2O_3, and CeO_2) in the formation of NO and put forward a Mars–Van Krevelen mechanism.

This study focuses on the oxidation of ammonia over a $LaCoO_3$ perovskite. This is a typical mixed oxide with a rhombohedral distortion of the cubic lattice structure. It has been studied for the combustion of hydrocarbons and organic compounds [13,14] de-NO_x [15] and hydrogenation [16,17]. Moreover, ammonia oxidation over $LaCoO_3$ has shown good results [3,7,11].

The temporal analysis of products or TAP [18–21] has been recognized as an important transient experimental method for heterogeneous catalytic reaction studies. It is especially suited to the study of fast highly exothermic reactions, due to the small amounts of reactants used and the operation in the diffusion regime which eliminates all external mass transfer limitations [18]. TAP analysis gave insights into the reaction mechanism of high temperature reactions, such as ammonia oxidation [12,22–24], methane partial oxidation [25] and HCN production over platinum [26,27].

2. Experimental

2.1. Catalyst synthesis and characterization

$LaCoO_3$ has been synthesized by a modified citrate gel method. $La(NO_3)_3{\cdot}6H_2O$ (Sigma–Aldrich, 99.9%), $Co(NO_3)_2{\cdot}6H_2O$ (Fluka, 98%) and citric acid (Riedel-de Haën 99.5%) were used as precursors.

Both nitrate salts are dissolved separately into a minimum amount of water. Citrate acid is added (molar ratio citric acid/metal = 2/1) to the cobalt nitrate solution to form a citrate complex with the cobalt while stirring at room temperature. Then the lanthanum solution is added and the pH is kept at 6.5–7 by using pure ammonia to form the sol. The sol is slowly evaporated at 353 K until a viscous gel is formed. The gel is dried at 433 K to evacuate NO_x from the material.

Calcination is done in two steps: first at 873 K under air in a muffle furnace in order to oxidize all the organic compounds for 6 h. To further optimize the crystal structure of the material, a second calcination is performed in a tubular quartz cell at 1273 K under flowing O_2 (gas flow rate of 75 ml min^{-1}) for 10 h.

X-ray diffraction (XRD) patterns were recorded using a Bruker D5005 diffractometer and Cu Kα radiation with 0.02° (2θ) steps over the 3–80° angular range. The crystal phase was determined by simulating and fitting the experimental XDR patterns using the Rietveld method [28]. The specific surface areas were determined by the BET method using nitrogen adsorption at 77 K (Micromeritics ASAP 2020). The samples were, before analysis, degassed under vacuum for 6 h.

Chemical analysis was determined by atomic emission using an induced plasma technique (ICP) (Activa Horiba). Scanning electron microscopy (SEM) analysis (Jeol JSM 5800LV) was applied to determine the grain size of the samples and the thickness of the coated layers. In the last case, the tubes were cut with a diamond saw.

2.2. Temporal analysis of products experiments

Transient experiments have been performed in the TAP-2 reactor system [19,20] over $LaCoO_3$ at 973 K. A TAP pulse response experiment consists of injecting a very small amount of gas per pulse into a tubular fixed-bed reactor that is kept under vacuum. In fact, the reactor is placed on top of a vacuum chamber containing a large diffusion pump and the reactor exit is continuously evacuated. The number of molecules that were admitted per pulse varied between 5 and 20 nmol.

The pressure rise in the micro-reactor is small, and the gas molecules move through the reactor bed mainly by Knudsen diffusion. The time-dependent exit flow of each gas is detected by a quadrupole mass spectrometer.

A weight of 25 mg of catalyst (sieve fraction between 150 and 200 μm) was loaded in a quartz reactor (40 mm length and 3 mm internal diameter) between two layers of SiC (200 μm).

Two kinds of transient experiments were performed over the sample at 973 K: multipulses of ammonia (NH_3:Ar = 1:5), oxygen (O_2:CF_4 = 1:1), labeled oxygen ($^{18}O_2$), nitrous oxide (N_2O:Ar = 1:1), or nitric oxide (NO:Ar = 1:5) and pump probe experiments, consisting of pulses of one reactant followed by another one at different time delays (depending on the experiment between 0.2 and 3 s). Pump probe experiments have been carried out with several gas mixtures: ammonia/oxygen, ammonia/labeled oxygen, nitrous oxide/oxygen, NO/ammonia, $^{15}N^{18}O$/ammonia. Before each experiment, the sample was pre-treated by a series of pulses of O_2 until a stable oxygen pulse response was observed. Ammonia strongly adsorbs not only on the catalysts but also on colder parts of the reactor system. A very broad ammonia pulse is obtained, often too small for correct quantification. Therefore, no ammonia pulse responses are reported and the conversion is estimated from the production of NO and N_2.

2.3. $^{16}O_2/^{18}O_2$ exchange experiments

The oxygen exchange experiments were carried out in a fixed-bed reactor containing 50 mg of sample at 1023 K. A gas mixture of 200 mL min^{-1} of 2% $^{16}O_2$ + 4% He + 94% Ar was replaced by a mixture of 200 mL min^{-1} of 2% $^{18}O_2$ + 98% Ar. After this experiment, a back switch was performed. The changes in the gas composition were continuously monitored by a mass spectrometer (m/e = 32, 34, 36, 40 & 4). Helium was added to the feed gas as an inert tracer.

2.4. Steady-state experiments

The catalyst was tested under continuous flow conditions in an annular fixed-bed quartz reactor. The catalyst is coated on a mullite tube that at the same time serves as a thermocouple well. The mullite tube has an external diameter of 3 mm and is placed concentrically inside a quartz tube with an internal diameter of 4 mm. The gas flows around the catalyst in the annular space. This reactor configuration is well adapted for fast reactions with strong thermal effects [29]. Due to the low flow resistance, high space velocities can be applied resulting in very short contact times. The reactor was placed inside a tubular furnace. The bed temperature was measured with a thermocouple placed inside the mullite tube measuring directly the catalyst temperature.

Before coating the catalyst on the mullite tube, this specific zone of the mullite tube was treated with diluted HF (10vol%) for 2 h at room temperature to remove silica from the mullite and thus increase the porosity to enhance the coating adherence. Afterward the tube is rinsed thoroughly and heated to 773 K for 2 h to remove the epoxy resin that was used to protect the part of the tube that is to stay free of catalyst coating. Typical suspensions were prepared by mixing 3.96 g of water with 1 g of catalyst and 0.04 g of acetic acid (AA) and 0.7 wt.% of Tylose® MH 300 P2 (methylhydroxyethyl cellulose, MW = 95 000, Clariant) as binder [30]. The suspension is heated at 323 K for 10 min and then cooled down to room temperature and stirred for 24 h. The slurry is deposited on the mullite tube with a syringe, while keeping the tube under horizontal rotation (2000 rpm). It is well known that cobalt can diffuse into ceramic supports at high temperatures. Therefore, a first layer of cobalt oxide was deposited on the mullite tube and kept at 1173 K overnight. Then, approximately 1.5 mg of the $LaCoO_3$ perovskite was deposited onto the cobalt oxide layer. The length of the layer is 1 cm and its thickness is estimated at approximately 30 μm by

Table 1
The sign of the variation of the independent variable with respect to the main observables. The range of operating conditions is given in parentheses.

	L/F (220–3300 m s mol^{-1})	T (960–1125 K)	Y_{O_2} (0.1–0.4)	Y_{NH_3} (0.01–0.05)
S_{NO_x} (0.82–0.98)	–	–	–	+
S_{N_2O} (0–2600 ppm)	–	–	–	+
X_{NH_3} (0.25–0.67)	+	+	0	0

Y_{O_2}, Y_{NH_3}, the mol fraction of oxygen and ammonia, respectively (mol/mol)

SEM observation of the transversal section. Two tubes have been prepared and tested with good reproducibility. Due to the absence of any porosity, only the outer surface of the catalyst layer participates to the reaction. This has been verified experimentally by varying the layer thickness and its effect on the conversion and selectivity. In analogy with a fixed-bed reactor (W/F_{NH_3}), the kinetic data are represented by L/F_{NH_3}, where L stands for the length of the catalyst coating and F_{NH_3} is the molar flow rate of ammonia.

Standard conditions consisted of a mixture of 3 vol.% NH_3 and 20 vol.% O_2 at a total flow rate of 400 ml min^{-1}. CF_4 was added to the mixture as an internal calibration standard. A large range of conditions has been investigated, as indicated in Table 1. Analysis of reactants and products was performed on-line with an IR spectrometer equipped with a light-pipe (Nicolet 380 with a spectral resolution of 1 cm^{-1}). This allowed the quantitative analysis of NH_3, NO, NO_2, N_2O, H_2O and CF_4. After dissolving NH_3, NO_x in water the effluent was passed through a Peltier-type condenser and fed to a micro GC (Agilent M200). The micro GC contained a molsieve (MS5A) and Poraplot Q column to analyze N_2, O_2, H_2, N_2O and CF_4. In this way, correct O, N and H balances were obtained (less than 5% deviation).

We report here the selectivity to NO_x, the sum of NO and NO_2, although both gases have been analyzed independently by the IR spectrometer. A gas-phase reaction occurs between NO and NO_2 due to the presence of oxygen in the effluent gas. This reaction will continue in the transfer lines from the reactor to the analyzer and depends on the flow rate. Moreover, during TAP experiments at very low pressure, the equilibrium is shifted to NO and no significant amount of NO_2 is detected.

3. Results

3.1. Catalyst characterization

The chemical composition of the materials determined by ICP was not fully in agreement with the nominal composition. This is probably due to a small loss of cobalt oxide by sublimation during calcination. Lanthanum was found in excess in the material in the form of $La(OH)_3$.

The XDR showed that the synthesized material consists of a perovskite phase with a rhombohedral structure. The diffractogram is shown in Fig. 1. The diffractogram indicates the presence of lanthanum hydroxide and Rietveld quantification attributed it to 5 wt.%.

Textural characterization by N_2 adsorption has shown a very low specific surface area of 2.4 m^2/g. Crystallite sizes between 200 and 600 nm were observed by SEM for the well-crystallized sample.

3.2. Steady-state performance

Fig. 2 shows the ammonia conversion and the selectivity to the N-containing products as a function of the temperature. The NO selectivity is rather constant between 973 and 1073 K and then drops significantly at higher temperatures. A rather low N_2O selectivity of 2% is observed at 973 K that decreases below the detection limit at 1073 K. On the contrary, the nitrogen selectivity increases with temperature. The effect of the operation conditions on the NO_x and N_2O selectivity and the ammonia conversion are summarized in Table 1. This table gives the sign of the variation of the independent variable on the main observables as well as the range of operating conditions. Thus, increasing the L/W increases the ammonia conversion but lowers the NO_x and N_2O selectivity. In fact, the NO_x selectivity decreases very little with increasing ammonia conversion from 0.25 to 0.65, less than 1% at isothermal conditions. The N_2O selectivity drops from 1500 to 1000 ppm at 1073 K and 3 mol% of ammonia. The effect of the operating variables has been conducted over a small range of ammonia conversions at isothermal conditions. Increasing the oxygen partial pressure lowers the NO_x and N_2O selectivity but does not influence the ammonia conversion. Increasing the ammonia partial pressure increases the NO_x and even more the N_2O selectivity. However, no clear effect of the ammonia partial pressure on the ammonia conversion has been observed. This might be due to the strong adsorption of ammonia on the catalyst as observed during TAP experiments. Although no specific long-term stability test have been performed, reproducible data under standard test conditions were obtained even after several days of time on stream.

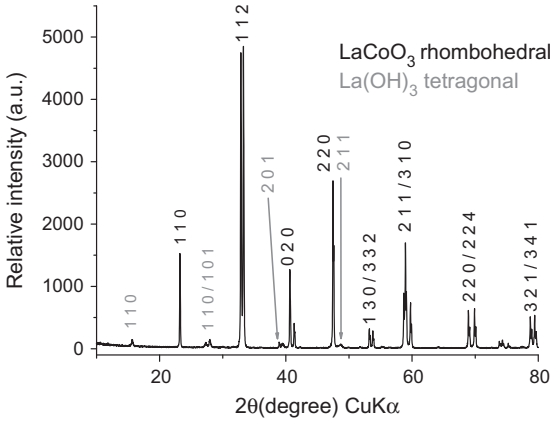

Fig. 1. X-ray diffraction pattern of the synthesized $LaCoO_3$ perovskite.

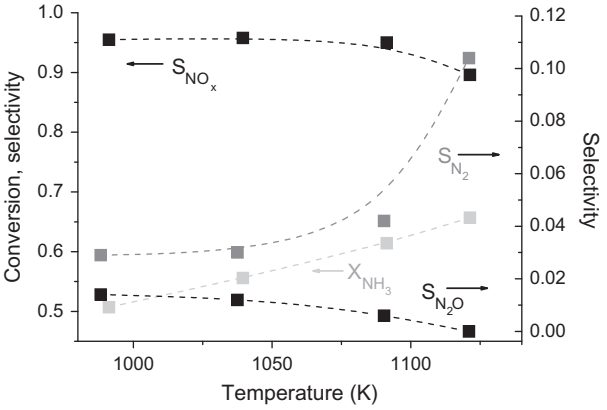

Fig. 2. NH_3 conversion and NO_x, N_2O and N_2 selectivity over $LaCoO_3$ as a function of the catalyst temperature in an annular reactor (3% NH_3, 20% O_2, 77% Ar, flow rate of 400 ml min^{-1}).

3.3. Oxygen interaction with $LaCoO_3$

No oxygen release was recorded when the $LaCoO_3$ sample was heated without further treatment to 973 K under vacuum. Then a

series of 400 oxygen pulses was admitted. The integrated area under the oxygen pulse response is plotted against the number of oxygen pulses in Fig. 3. No oxygen has been detected at the reactor exit during the first 40 pulses. Then a breakthrough of oxygen is observed that levels off after 90 pulses. Even when the oxygen pulse response is stable toward the end of the series, the pulse response is broad indicating a strong interaction of oxygen with the perovskite. When the pulsing of oxygen was stopped, a continuous signal of oxygen desorbing from the sample was observed. Reintroducing oxygen pulses resulted in a renewed oxygen uptake depending on the time the sample was kept under vacuum.

The total amount of oxygen that has been adsorbed by the sample estimated from Fig. 3 corresponds to approximately 0.5 μmol of O atoms, which is equal to 8 μmol/m^2 by using the measured BET area of 2.4 m^2/g. This is in good agreement with the data of Royer et al. [31] who reported an oxygen storage capacity for $LaCoO_3$ of 12 μmol/m^2 at 603 K.

To further investigate the oxygen adsorption mechanism, $^{18}O_2$ was pulsed over the sample. The first transient responses of the oxygen isotopomers as well as those after pulsing $^{18}O_2$ for 30 min are shown in Fig. 4a. A small response of $^{18}O_2$ is observed due to its large conversion and the main product is $^{16}O_2$. After 30 min of pulsing $^{18}O_2$, the $^{18}O_2$ response has increased just like the $^{16}O^{18}O$ response and the $^{16}O_2$ response has decreased slightly but remains the main product. Fig. 4b shows the normalized responses of the oxygen isotopomers. The normalized responses of the products $^{16}O^{18}O$ and $^{16}O_2$ are rather similar, while the reactant $^{18}O_2$ normalized response is very narrow.

The total amount of exchangeable oxygen can be determined from labeled oxygen exchange experiments under flow conditions. The data are shown in Fig. 5. The $^{16}O^{18}O$ response increases slowly, then goes through a maximum and slowly decreases. The $^{18}O_2$ increases even slower and levels off after 600 s. From these data, it is estimated that approximately 90% of the oxygen in the perovskite has been exchanged with gas-phase oxygen.

3.4. Ammonia interaction with $LaCoO_3$

After a series of 100 oxygen pulses, a series of ammonia pulses has been carried out and the products have been recorded (not shown). The main product was NO, followed by N_2. The NO selectivity amounted to 92%. A small signal at $m/e = 44$ has been observed, which is attributed to N_2O. The formation of NO decreased slowly while the N_2 formation increased with the number of NH_3 pulses. After a very long series of NH_3 pulses, the formation of hydrogen was observed. Probably at this stage, the catalyst is in a too reduced state, which is no longer representative for the selective ammonia oxidation. The data reveal the participation of oxygen from the perovskite into the oxidation of ammonia, as no gas-phase oxygen was supplied during this experiment. Afterward a re-oxidation of the catalyst resulted in an oxygen uptake and restored the initial NO selectivity when pulsing NH_3. A broad NO signal indicates that NO strongly adsorbs on $LaCoO_3$.

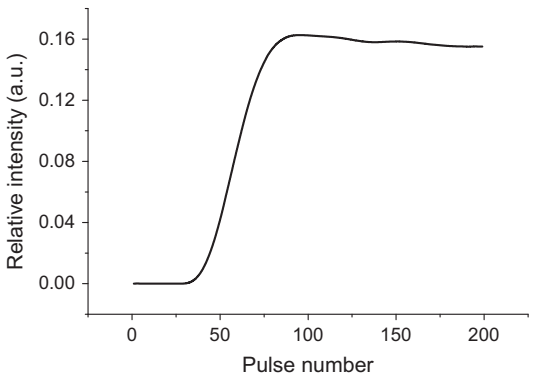

Fig. 3. Integrated O_2 pulse response (~10 nmol O_2 & 10 nmol Ar per pulse) as a function of the pulse number.

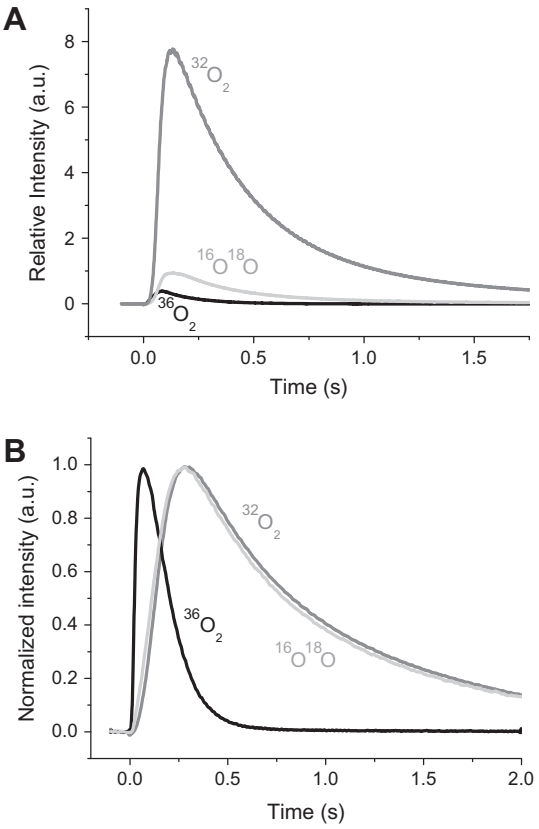

Fig. 4. (A) Pulse responses of $m/e = 36$, 34 and 32 from a pulse of $^{36}O_2$ over $LaCoO_3$ at 973 K. (B) Height normalized pulse responses of $m/e = 36$, 34 and 32 from a pulse of $^{36}O_2$ over $LaCoO_3$ at 973 K. For clarity reasons, only the first part of the pulse is shown.

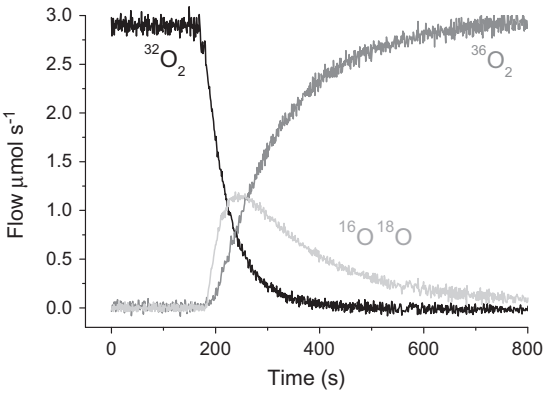

Fig. 5. Exit flows as a function of time for an isotopic oxygen exchange experiment over $LaCoO_3$ perovskite at 1023 K.

3.5. Pump–probe experiments

The effect of gas-phase oxygen on the ammonia oxidation was further investigated by pump–probe experiments. Fig. 6 gives an example for the main product responses on an ammonia/oxygen and an oxygen/ammonia pump–probe experiments with a time delay between the two pulses of 3 s. This delay has been varied

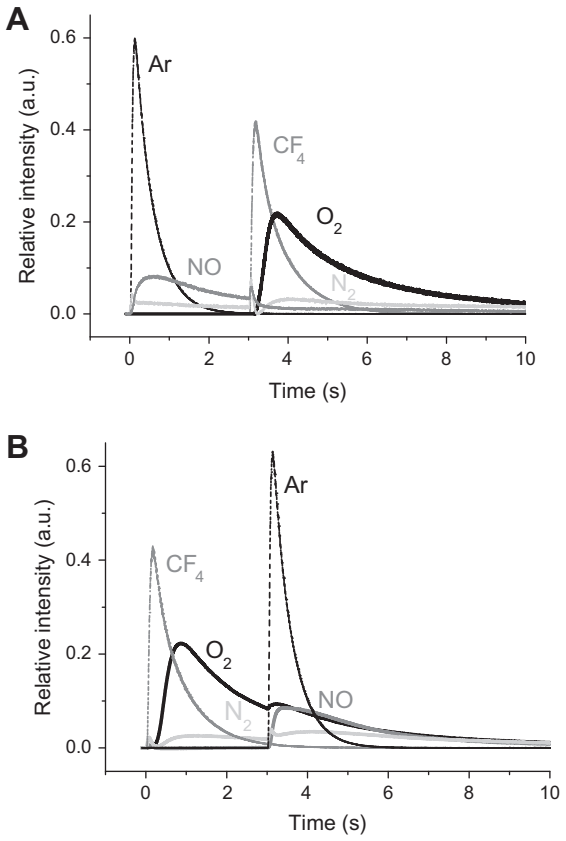

Fig. 6. (A) NO, N_2 and O_2 pulse responses of a NH_3–O_2 pump–probe with a 3 s delay at 973 K. (B) NO, N_2 and O_2 pulse responses of a O_2–NH_3 pump–probe with a 3 s delay at 973 K.

and the effect on the product distribution is shown in Fig. 7. Fig. 6 shows that NO is the main product formed on the ammonia pulse and N_2 the main product formed on the oxygen pulse. Note that ammonia adsorbs strongly and NH_x species will be present longer than the time-scale of the pump–probe experiment. In fact upon introduction of the oxygen pulse after the ammonia pulse, the NO response drops quickly and after a delay a renewed NO formation can be observed. On both pump–probe experiments, the nitrogen response consists of a first narrow peak followed by a broader signal. A very small signal at $m/e = 44$ was observed on the oxygen pulse. In this case, its attribution to N_2O is not unambiguous as it can also be attributed to CO_2 formed by oxidation of carbon that might be present on the catalyst. For this reason and the fact that the signal is very small and noisy, the transient response is not shown in Fig. 6. The $m/e = 28$ response could be attributed to nitrogen as the signal intensity was much larger than the $m/e = 44$ signal and the formation of CO could be discarded by comparing the responses at $m/e = 14$ and 12.

The NO selectivity has been calculated assuming that NO and N_2 are the only nitrogen containing products formed and taking into account the amounts on both the NH_3 and O_2 pulse. The NO selectivity in these pump–probe experiments varied between 90% and 95% while the ammonia conversion was estimated at approximately 75%. When increasing the time delay between the ammonia pulse and the oxygen pulse, the ammonia conversion and NO and N_2 yields are hardly affected.

Pulses of N_2O over $LaCoO_3$ are readily converted into nitrogen, with a conversion of more than 95%. No significant amount of oxygen is detected indicating that the catalyst retains the extracted oxygen atom. To investigate the oxidation state of $LaCoO_3$ on the N_2O decomposition, O_2/N_2O pump–probe experiments were conducted. Fig. 8 shows that the N_2O concentration decreases (thus the N_2O conversion increases) while the N_2 formation increases with the increasing time delay between the oxygen and N_2O pulse. Changing the time delay from 0.5 to 2.0 increases the conversion from 85% to 93%. Thus, the lower the oxidation degree of the catalyst is, the faster is the N_2O decomposition rate.

The decomposition of NO is much less than N_2O. Conversions less than 2% were observed for NO pulses over $LaCoO_3$. Again no oxygen release has been observed. On the other hand, pulses of labeled $^{15}N^{18}O$ are almost completely converted into mainly $^{15}N^{16}O$. Thus, $LaCoO_3$ is capable of exchanging its oxygen atoms with those of nitric oxide. Again the influence of the oxidation state of the catalyst on the NO decomposition has been studied by pump–probe experiments. In this case, the time delay in the pump–probe experiment had hardly any effect on the rate of the NO decomposition.

The interaction between ammonia and nitric oxide was studied by $NH_3/^{15}N^{18}O$ pump–probe experiments. On the NH_3 pulse, the formation of NO was observed and on the $^{15}N^{18}O$ pulse the formation of $^{15}N^{16}O$ ($m/e = 31$), $^{15}N_2 + NO$ ($m/e = 30$) and $^{15}N^{14}N$ ($m/e = 29$). Due to the overlap of NO and $^{15}N_2$ of the $m/e = 30$ response, the quantification of the product distribution during this experiment is not too accurate. An approximate ratio of $^{15}N_2$ to $^{15}N^{14}N$ of 3 is estimated, which is not significantly different than the ratio of ^{15}NO to ^{14}NO on the $^{15}N^{18}O$ pulse.

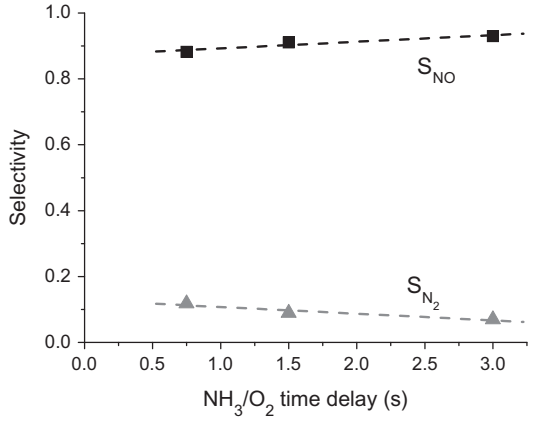

Fig. 7. Effect of the time delay between NH_3 and O_2 during a pump–probe experiment on the NO and N_2 selectivity at 973 K.

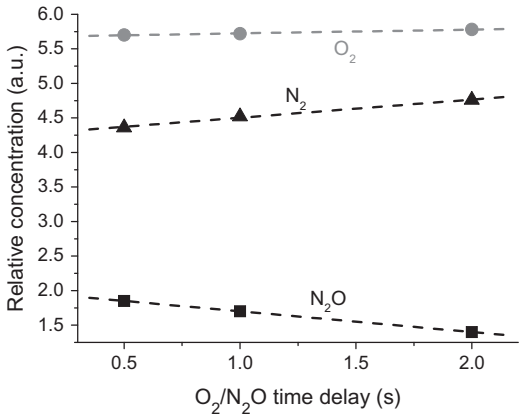

Fig. 8. Effect of the time delay between O_2 and N_2O during a pump–probe experiment on the concentrations of N_2O, O_2 and N_2 at 973 K.

4. Discussion

The high temperature ammonia oxidation has been mainly studied over platinum experimentally [22–24,32–37] and theoretically [38–40] but in a lesser extent over metal oxides [3,9,10,12] Few studies in the literature [3,11] report on the reaction mechanism of ammonia oxidation at high temperatures over perovskites.

In the recent literature, it is generally admitted that the main features for the ammonia oxidation over platinum consist of an oxidative stepwise dehydrogenation of adsorbed ammonia assisted by oxygen adatoms or adsorbed hydroxyl groups [38,40,41]. The proposed mechanisms include steps for the recombination of nitrogen adatoms with oxygen adatoms to NO and recombination of two nitrogen adatoms to nitrogen. Nitrous oxide is formed by the reaction between NO and nitrogen adatoms. Novell-Leruth et al. [40] showed by DFT calculations over Pt(1 0 0) that the oxidative dehydrogenation route is far more favorable than a route through nitroxyl (HNO) or hydroxylamine (NH_2OH) intermediates.

Although the ammonia oxidation over platinum and $LaCoO_3$ perovskite has many features in common (e.g. the product distribution as a function of temperature), there exist many differences as well (e.g. the side reactions involving NO and N_2O; the NO selectivity dependence on P_{O_2}). This is likely due to the difference in the surface between platinum and $LaCoO_3$, the latter exposing mainly oxygen atoms with a small amount of oxygen vacancies [42]. Thus, a different interaction with the reactants and products can be expected and the occurrence of different reaction intermediates. In the case of ammonia oxidation over oxides, nitroxyl or hydroxylamine intermediates are most often proposed [11,37,43]. This is in line with observations of these intermediates by infrared spectroscopy at low temperatures [44,45]. Moreover, Brűggemann and Keil [46] have established a reaction mechanism based on nitroxyl or hydroxylamine intermediates for the oxidation of ammonia over HZSM-5 by DFT. Accordingly, the reaction mechanism proposed here involves nitroxyl or hydroxylamine intermediates, although no direct evidence exists for these species at high temperatures on perovskites.

$LaCoO_3$ contains oxygen vacancies ($V^{\cdot\cdot}_{Os}$) as well as electronic point effects ($h^{\cdot}$, e') that allow for a finite compositional variation, $LaCoO_{3-\delta}$, governed by the oxygen partial pressure [47]. In this study, the interaction of ammonia with a $LaCoO_3$ perovskite has been investigated at different degrees of its oxidation state by varying the oxygen gas phase partial pressure. Before presenting a reaction mechanism, the main reaction paths are summarized first.

Ammonia readily reacts over a pre-oxidized sample without gas-phase oxygen into mainly ~90% NO, ~5% N_2 and a small amount of N_2O. Thus, the reaction between adsorbed ammonia with surface oxygen from the sample seems to be the principal reaction route at steady-state conditions. The surface oxygen at the surface can be replenished by the diffusion of oxygen from the bulk or by supplying gas-phase oxygen. The reaction proceeds by a Mars and Van Krevelen mechanism. This is confirmed by changing the time delay between the oxygen and ammonia in the pump–probe experiments. The conversion expressed as the sum of NO and N_2 formed remains constant with the time delay. If no gas-phase oxygen is supplied, the catalysts will be more and more reduced by the ammonia conversion and the selectivity to nitrogen increases. A fast gas-phase oxygen activation on the catalyst to minimize the number of reduced sites is thus crucial for a good NO selectivity. Pérez-Ramírez and Kondratenko [12] also attributed a Mars and Van Krevelen mechanism for the ammonia oxidation over Cr_2O_3, CeO_2 and Fe_2O_3, although only the latter oxide showed participation of bulk oxygen.

However, pump–probe TAP experiments show an increased N_2 production at the moment of the introduction of gas-phase oxygen. One might thus postulate the presence of a reactive oxygen surface species that favors N_2 formation. This illustrates the importance of the catalyst oxidation state and the presence of reactive oxygen surface species on the NO selectivity. Thus we examine the oxygen activation over $LaCoO_3$ in more detail using the labeled oxygen exchange experiments.

The theory of isotopic oxygen exchange is well developed and three classes of exchange mechanisms are known:

The first mechanism is the equilibration reaction, which requires no participation of oxygen atoms from the solid, referred to as R^0:

$$^{16}O_{2(g)} + {}^{18}O_{2(g)} \rightleftharpoons 2\,{}^{18}O{}^{16}O_{(g)} \quad (1)$$

The second mechanism constitutes a simple heteroexchange involving only one solid oxygen atom (R^1):

$$^{18}O_{2(g)} + {}^{16}O_{(s)} \rightleftharpoons {}^{18}O{}^{16}O_{(g)} + {}^{18}O_{(s)} \quad (2)$$

$$^{18}O{}^{16}O_{(g)} + {}^{16}O_{(s)} \rightleftharpoons {}^{16}O_{2(g)} + {}^{18}O_{(s)} \quad (3)$$

The third reaction mechanism involves the exchange of two oxygen atoms of the solid simultaneously (complex heteroexchange, R^2):

$$^{18}O_{2(g)} + 2\,{}^{16}O_{(s)} \rightleftharpoons {}^{16}O_{2(g)} + 2\,{}^{18}O_{(s)} \quad (4)$$

$$^{16}O_{2(g)} + {}^{18}O_{(s)} + {}^{16}O_{(s)} \rightleftharpoons {}^{18}O{}^{16}O_{(g)} + 2\,{}^{16}O_{(s)} \quad (5)$$

The first mechanism can be excluded under TAP conditions as collisions between gas-phase molecules can be neglected in the Knudsen diffusion regime. TAP data allow easy discrimination between R^1 and R^2 as the primary and secondary products of these two reaction mechanisms are different. For the case of oxygen exchange over $LaCoO_3$, shown in Fig. 3, $^{32}O_2$ is the main product. Moreover, the normalized response of $^{16}O^{18}O$ is broad, indicating it is a secondary product and not a primary product (in which case it would resemble more the shape of the $^{36}O_2$ normalized response). Because the ^{18}O fraction on the surface is very small, the consecutive reaction step (5) is rather slow thus hardly narrowing the response of $^{32}O_2$. Thus, the complex heteroexchange R^2 mechanism is the dominant mechanism. However, the slight delay in the normalized $m/e = 32$ signal compared to the $m/e = 34$ implies a small contribution of the simple exchange mechanism (R^1).

The oxygen exchange flow experiments can be analyzed along the lines detailed in Sadovskaya et al. [48]. Applying this analysis to the oxygen flow data over $LaCoO_3$, no distinction can be made between the mechanisms R^1 and R^2 as the surface reaction is much faster than the bulk diffusion. However, the TAP data show that the R^2 mechanism dominates. Royer et al. estimated an activation energy of approximately 76 kJ/mol for the initial ^{18}O exchange over $LaCoO_3$ [49].

In conclusion, oxygen chemisorbs on the surface and exchanges rapidly both atoms with those of the surface, after dissociation and oxygen diffusion through the bulk is the rate-controlling step for further exchange.

For perovskites having the general formula ABO_3, the following global redox reaction takes place [11,50]

$$4B^{n+} + 2V_O + O_2(g) = 4B^{(n+1)+} + 2O^{2-} \quad (6)$$

This redox reaction is a four electron process and has been extensively studied over a lot of different oxide materials [47,51]. It consists of the following elementary steps, here given in Kröger–Vink notation [51,52]:

$$\text{adsorption}: O_2 + V^{\cdot\cdot}_{O_s} + e' = (O_2)^{\cdot}_{O_s} \quad (7)$$

$$\text{dissociation}: (O_2)^{\cdot}_{O_s} + V^{\cdot\cdot}_{O_s} + e' = 2O^{\cdot}_{O_s} \quad (8)$$

$$\text{incorporation}: O^{\cdot}_{O_s} + V^{\cdot\cdot}_{O_b} + e' = O^{X}_{O_b} + V^{\cdot\cdot}_{O_s} \quad (9)$$

$$\text{redox couple}: Co'_{Co} = Co^{X}_{Co} + e' \quad (10)$$

Eqs. (7)–(9) show that several surface oxygen species can co-exist on the surface: physisorbed O_2, superoxide (O_2^-), peroxide (O^-) and surface lattice oxygen (O^{2-}) [51]. Furthermore, the adsorption of oxygen on $LaCoO_3$ requires two vacancies that are each associated with two cobalt cations. Cobalt cations can present two redox couples: Co^{4+}/Co^{3+} and Co^{3+}/Co^{2+}. The first redox couple is proposed in A′ substituted perovskites [50] and is typically associated with the α-desorption peak in the oxygen TPD [53]. The second couple is proposed for $LaCoO_3$ and associated with β-desorption peak [50,53]. This desorption peak is observed above 1000 K and thus corresponds well with the temperature range used for the ammonia oxidation.

Based on the active site for oxygen activation and the nitroxyl intermediate described above, the following reaction route to NO, the main product observed experimentally, is proposed:

$$NH_{3,ads} + O^X_{O_s} \rightarrow H_2NOH^X_{O_s} \quad (11)$$

$$H_2NOH^X_{O_s} + O^X_{O_s} \rightarrow HNO^X_{O_s} + H_2O + V^{\cdot\cdot}_{O_s} + 2e' \quad (12)$$

$$HNO^X_{O_s} + O^X_{O_s} \rightarrow NO^{\cdot}_{O_s} + OH^{\cdot}_{O_s} + e' \quad (13)$$

$$NO^{\cdot}_{O_s} \rightarrow NO_{(g)} + V^{\cdot\cdot}_{O_s} + e' \quad (14)$$

$$2OH^{\cdot}_{O_s} \rightarrow H_2O_{(g)} + O^X_{O_s} + V^{\cdot\cdot}_{O_s} + e' \quad (15)$$

$$5Co^X_{Co} + 5e' \rightarrow 5Co'_{Co} \quad (16)$$

$$NH_{3,ads} + 2.5O^X_{O_s} + 5Co^X_{Co} \rightarrow NO_{(g)} + 1.5H_2O_{(g)} + 2.5V^{\cdot\cdot}_{O_s} + 5Co'_{Co} \quad (17)$$

The subscript ads in steps (11)–(17) refers to physisorbed or chemisorbed species. Ammonia probably adsorbs through interaction of its lone electron pair on the nitrogen atom with a cation on the surface. This will weaken the N–H bond and oxygen insertion will become possible followed by a dehydrogenation steps to give a nitroxyl HNO species. The alternative route would be first a dehydrogenation step to give NH_{ads} species followed by oxygen insertion yielding the same nitroxyl species. The last dehydrogenation step then leads to NO^- that desorbs as NO. The electroneutrality is established by the change in oxidation state of the cobalt cations (step (16). Thus steps (11)–(15) are accompanied by five Co^{3+}/Co^{2+} redox changes. The surface oxygen vacancies ($V^{\cdot\cdot}{}_{Os}$) are annihilated by either bulk diffusion or by gas-phase oxygen (steps (7)–(9)). Steps (11)–(15) are not elementary steps, as the oxidizing species cannot be the surface anions O^{2-} (due to its −2 oxidation state), but rather singly or doubly ionized anionic vacancies [54]. This process occurs through electron transfer that is expected to occur rapidly due to the good electrical conductivity of $LaCoO_3$ [50,51]. The net reaction is an incorporation of surface lattice oxygen into the NO molecule, according to the Mars and Van Krevelen mechanism.

The formation of N_2O takes place by the recombination of two nitroxyl species:

$$2HNO^X_{O_s} \rightarrow N_2O_{(g)} + H_2O \quad (18)$$

Over platinum N_2O formation has been proposed by the combination of two adsorbed NO species [55,56]. On the contrary to platinum, over $LaCoO_3$ no N_2O formation has been observed when pulsing NO. Reaction (18) is proposed over different oxides [37,43] and is in analogy with hyponitrous acid decomposition [57]. Cheskis et al. [58] experimentally studied the decay rates of HNO in the gas phase. They mainly found N_2O as a product and concluded that the reaction of two HNO molecules leads directly to this product by hydrolysis.

N_2O can then be decomposed into N_2, involving an oxidation of an oxygen vacancy site:

$$N_2O_{(g)} + V^{\cdot\cdot}_{O_s} + e' \rightarrow O^{\cdot}_{O_s} + N_{2(g)} \quad (19)$$

Step (19) explains the dependence of the rate of N_2O decomposition on the oxidation state of the surface, as observed experimentally (Fig. 8), as the higher the oxidation state the lower the surface oxygen vacancy concentration.

To account for the additional nitrogen production on the oxygen pulse during a O_2/NH_3 pump–probe experiment, the following steps are added to the reaction mechanism:

$$NH_{3,ads} + O^{\cdot}_{O_s} \rightarrow NH_{2,ads} + OH^{\cdot}_{O_s} \quad (20)$$

$$NH_{2,ads} + O^{\cdot}_{O_s} \rightarrow NH_{ads} + OH^{\cdot}_{O_s} \quad (21)$$

$$NH_{ads} + HNO^X_{O_s} \rightarrow N_{2(g)} + H_2O_{(g)} \quad (22)$$

In step (20), adsorbed ammonia reacts with an oxygen surface species (peroxide), formed in step (8), rather than with a lattice oxygen species. The surface lifetime of the surface oxygen species is very short. The NH_{ads} species then are further reduced by NHO_{ads} species to form nitrogen (step (22)). Rather than a peroxide species, the reactive oxygen species could be a superoxide.

This reaction mechanism addresses the product distribution (NO, N_2O, N_2) as a function of the degree of oxidation of the catalyst surface. Over an oxidized surface, the selectivity to NO will be very high as the nitroxyl HNO intermediate species will react with lattice oxygen to yield NO, rather than a second-order reaction between two nitroxyl HNO species to N_2O. The decomposition of N_2O requires an oxygen vacancy, thus a partly reduced surface. Similarly, the formation of N_2 by step (22) is a second-order process, thus favored at high ammonia partial pressures. The catalyst surface must enable fast oxygen incorporation into its vacancies to minimize the formation of superoxide or peroxide species. The oxygen exchange experiments (Fig. 5) show that this is indeed the case.

A third route for the formation of N_2 is through the decomposition of NO, as observed by pulsing NO over the $LaCoO_3$. Teraoka et al. [50] studied the NO decomposition of NO over $La_{0.8}Sr_{0.2}CoO_3$ in a fixed-bed flow reactor. They observed an inhibition by oxygen on the NO decomposition rate. They proposed a reaction mechanism where NO chemisorbs on two adjacent surface oxygen vacancies followed by the formation of dinitrogen. The vacancies are regenerated by desorption of molecular oxygen from the surface. This reaction mechanism corresponds well with the results presented here on the ammonia oxidation. Oxygen desorption is probably too slow to be observed on the time-scale of a TAP experiment. Thus, the following step can be added:

$$NO_{(g)} + V^{\cdot\cdot}_{O_s} + e' \rightarrow NO^{\cdot}_{O_s} \quad (23)$$

$$2NO^{\cdot}_{O_s} \rightarrow 2O^{\cdot}_{O_s} + N_{2(g)} \quad (24)$$

Moreover, by using labeled $N^{18}O$ oxygen scrambling with the perovskite has been observed, which can be represented as:

$$N^{18}O_{(g)} + {}^{16}O^X_{O_s} + V^{\cdot\cdot}_{O_s} + e' \rightarrow [{}^{16}O{-}N{-}{}^{18}O]^{\cdot}_{O_s} \rightarrow N^{16}O_{(g)} + {}^{18}O^X_{O_s} + V^{\cdot\cdot}_{O_s} + e' \quad (25)$$

This process resembles the simple oxygen exchange (step (2)). A possible mechanism is the adsorption of $N^{18}O$ with the oxygen atom into an oxygen vacancy site adjacent to a surface oxygen anion. Next, a nitrite $^{16}ON^{18}O^-$ intermediate species is formed that now can desorb as $N^{16}O$ (or $N^{18}O$).

The formation of $^{15}N^{14}N$ in small amounts ($^{15}N_2$:$^{15}N^{14}N$ = 3:1) during the $^{14}NH_3/^{15}NO$ experiments might indicate another, minor, formation route of nitrogen. Pérez-Ramírez et al. [23] proposed for the $^{15}N^{14}N$ formation over platinum a recombination of NH_x fragments with adsorbed NO. Because ^{14}NO is formed on the ammonia pulse, the $^{15}N^{14}N$ formation occurs probably through the $^{15}NO/^{14}NO$ decomposition reaction, rather than through the reaction with a NH_x fragment.

The steady-state results summarized in Table 1 support the reaction mechanism proposed here. The decrease of the NO_x and N_2O selectivity with increasing contact time indicates that these

are primary products that react to nitrogen in a consecutive step. Increasing the oxygen partial pressure or reducing the ammonia partial pressure has the same effect on the oxidation state of the surface and should have the same effect on the NO_x and N_2O selectivity, which is indeed the case. Under all conditions, oxygen is in excess and increasing the oxygen partial pressure will result in more reactive oxygen surface species that favor nitrogen formation rather than NO_x.

5. Conclusions

$LaCoO_3$ gives good selectivity to NO in the high temperature oxidation of ammonia. Nitrogen and nitrous oxide are side products. The low selectivity toward N_2O makes this catalyst a potential replacement of the PMG gauzes in industrial processes.

The reaction proceeds by a Mars and Van Krevelen mechanism. TAP experiments show that the dominant oxygen exchange mechanism takes place by the complex heteroexchange R^2.

NO and N_2O are formed through parallel routes from ammonia via surface nitroxyl (HNO) species. Formation of nitrogen occurs through at least three routes. Decomposition of the reaction products NO and N_2O gives N_2, the latter being the most reactive. The third route consists of the reaction of adsorbed ammonia with short-lived oxygen surface species, such as peroxide or superoxide species.

NO adsorbs into an oxygen vacancy and can form a nitrite ONO^- intermediate species through which it can exchange its oxygen atom with the perovskite surface.

The proposed reaction mechanism, mainly based on TAP experiments, is in good agreement with the observed steady-state trends.

Acknowledgment

This work was supported by TopCombi (NMP2-CT2005-515792) funded by the European Union.

References

[1] C.N. Satterfield, Heterogeneous Catalysis in Industrial Practice, second ed., Krieger Florida, 1996.
[2] J. Pérez-Ramírez, F. Kapteijn, K. Schöffel, J.A. Moulijn, Appl. Catal. B 44 (2003) 117.
[3] V.A. Sadykov, L.A. Isupova, I.A. Zolotarskii, L.N. Bobrova, A.S. Noskov, V.N. Parmon, E.A. Brushtein, T.V. Telyatnikova, V.I. Chernyshev, V.V. Lunin, Appl. Catal. A 204 (2000) 59.
[4] J. Petryk, E. Kolakowska, Appl. Catal. B 24 (2000) 121.
[5] J. Petryk, K. Schmidt-Szalowski, K. Krawczyk, Appl. Catal. A 175 (1998) 147.
[6] A.S. Noskov, I.A. Zolotarskii, S.A. Pokrovskaya, V.N. Kashkin, E.M. Slavinskaya, V.V. Mokrinskii, V.N. Korotkikh, Chem. Eng. J. 91 (2003) 235.
[7] L.A. Isupova, E.F. Sutormina, N.A. Kulikovskaya, L.M. Plyasova, N.A. Rudina, I.A. Ovsyannikova, I.A. Zolotarskii, V.A. Sadykov, Catal. Today 105 (2005) 429.
[8] M.M. Karavayev, A.P. Zasorin, N.F. Kleshchev, Khimia Moscow, 1983.
[9] B. Bernauer, A. Simecek, J. Vosolsobe, Czech. Chem. Commun. 47 (1980) 2097.
[10] B. Bernauer, A. Simecek, J. Vosolsobe, Czech. Chem. Commun. 47 (1980) 2087.
[11] Y. Wu, T. Yu, B.S. Dou, C.X. Wang, X.F. Xie, Z.L. Yu, S.R. Fan, L.C. Wang, J. Catal. 120 (1989) 88.
[12] J. Pérez-Ramírez, E.V. Kondratenko, J. Catal. 250 (2007) 240.
[13] H.G. Lintz, K. Wittstock, Catal. Today 29 (1996) 457.
[14] R.J.H. Voorhoeve, D.W. Johnson Jr, J.P. Remeika, P.K. Gallagher, Science 195 (1977) 827.
[15] M. Skoglundh, L. Löwendahl, K. Jansson, L. Dahl, M. Nygren, Appl. Catal. B 3 (1994) 259.
[16] P.R. Watson, G.A. Somorjai, J. Catal. 74 (1982) 282.
[17] J.O. Petunchi, J.L. Nicastro, E.A. Lombardo, J. Chem. Soc. Chem. Commun. (1980) 467.
[18] Y. Schuurman, Catal. Today 121 (2007) 187.
[19] J.T. Gleaves, G.S. Yablonskii, P. Phanawadee, Y. Schuurman, Appl. Catal. A 160 (1997) 55.
[20] J.T. Gleaves, J.R. Ebner, T.C. Kuechler, Catal. Rev. Sci. Eng. 30 (1988) 49.
[21] J. Pérez-Ramírez, E.V. Kondratenko, Catal. Today 121 (2007) 160–169.
[22] J. Pérez-Ramírez, E.V. Kondratenko, V.A. Kondratenko, M. Baerns, J. Catal. 227 (2004) 90.
[23] J. Pérez-Ramírez, E.V. Kondratenko, V.A. Kondratenko, M. Baerns, J. Catal. 229 (2005) 303.
[24] J. Pérez-Ramírez, E.V. Kondratenko, G. Novell-Leruth, J.M. Ricart, J. Catal. 261 (2009) 217.
[25] M. Fathi, F. Monnet, Y. Schuurman, A. Holmen, C. Mirodatos, J. Catal. 190 (2000) 439.
[26] V.A. Kondratenko, Appl. Catal. A 381 (2010) 74.
[27] S. Delagrange, Y. Schuurman, Catal. Today 121 (2007) 204.
[28] L.B. McCusker, R.B. Von Dreele, D.E. Cox, D. Louër, P. Scardi, J. Appl. Cryst. 32 (1999) 36.
[29] A. Beretta, P. Baiardi, D. Prina, P. Forzatti, Chem. Eng. Sci. 54 (1999) 765.
[30] G. Germani, A. Stefanescu, A.C. van Veen, Y. Schuurman, Chem. Eng. Sci. 62 (2007) 5084.
[31] S. Royer, H. Alamdari, D. Duprez, S. Kaliaguine, Appl. Catal. B 58 (2005) 273.
[32] A. Scheibe, M. Hinz, R. Imbihl, Surf. Sci. 576 (2005) 131.
[33] A. Scheibe, U. Lins, R. Imbihl, Surf. Sci. 577 (2005) 1.
[34] R. Imbihl, A. Scheibe, Y.F. Zeng, S. Gunther, R. Kraehnert, V.A. Kondratenko, M. Baerns, W.K. Offermans, A.P.J. Jansen, R.A. van Santen, PCCP 9 (2007) 3522.
[35] T. Pignet, L. Schmidt, Chem. Eng. Sci. 29 (1974) 1123.
[36] C.J. Weststrate, J.W. Bakker, E.D.L. Rienks, C.P. Vinoda, A.V. Matveevc, V.V. Gorodetskii, B.E. Nieuwenhuys, J. Catal. 242 (2006) 184.
[37] Il'Chenko, Golodets, J. Catal. 39 (1975) 57.
[38] W.K. Offermans, A.P.J. Jansen, R.A. van Santen, Surf. Sci. 600 (2006) 1714.
[39] G. Novell-Leruth, A. Valcarcel, A. Clotet, J.M. Ricart, J. Pérez-Ramírez, J. Phys. Chem. B 109 (2005) 18061.
[40] G. Novell-Leruth, J.M. Ricart, J. Pérez-Ramírez, J. Phys. Chem. C 112 (2008) 13554.
[41] R. Kraehnert, M. Baerns, Chem. Eng. J. 137 (2008) 361.
[42] S. Khan, R.J. Oldman, F. Cora, C.R. Catlow, S.A. French, S.A. Axon, Phys. Chem. Chem. Phys. 8 (2006) 5207.
[43] E.G. Vrieland, J. Catal. 32 (1974) 415.
[44] J.M.G. Amoresa, V.S. Escribanoa, G. Ramisb, G. Busca, Appl. Catal. B: Environ. 13 (1997) 45.
[45] D.W.L. Griffiths, H.E. Hallam, W.J. Thomas, J. Catal. 17 (1970) 18.
[46] T.C. Brűggemann, F.J. Keil, J. Phys. Chem. C 113 (2009) 13860.
[47] R. Merkle, J. Maier, Angew. Chem. Int. Ed. 47 (2008) 3874.
[48] E.M. Sadovskaya, Y.A. Ivanova, L.G. Pinaeva, G. Grasso, T.G. Kuznetsova, A. van Veen, V.A. Sadykov, C. Mirodatos, J. Phys. Chem. A 111 (2007) 4498.
[49] S. Royer, D. Duprez, S. Kaliaguine, J. Catal. 234 (2005) 364.
[50] Y. Teraoka, T. Harada, S. Kagawa, J. Chem. Soc. Faraday Trans. 94 (1998) 1887.
[51] S.B. Adler, X.Y. Chen, J.R. Wilson, J. Catal. 245 (2007) 91.
[52] P.J. Gellings, H.J.M. Bouwmeester, Catal. Today 58 (2000) 1.
[53] Y. Teraoka, M. Yoshimatsu, N. Yamazoe, T. Seiyama, Chem. Lett. (1984) 893.
[54] J.M. Herrmann, Catal. Today 112 (2006) 73.
[55] R. Burch, S.T. Daniells, P. Hu, J. Chem. Phys. 121 (2004) 2737.
[56] P. Denton, A. Giroir-Fendler, Y. Schuurman, H. Praliaud, C. Mirodatos, M. Primet, Appl. Catal. A: Gen. 220 (2001) 141.
[57] M.N. Hughes, Quart. Rev. Chem. Soc. 22 (1968) 1.
[58] S.G. Cheskis, V.A. Nadtochenko, O.M. Sarkisov, Int. J. Chem. Kinet. 13 (1981) 1041.